ACS APPLIED MATERIALS & INTERFACES

RESEARCH ARTICLE

www.acsami.org

Conjugated Fluorene Based Rod−Coil Block Copolymers and Their PCBM Composites for Resistive Memory Switching Devices

Shiang-Ling Lian,[†] Cheng-Liang Liu,[‡] and Wen-Chang Chen*[,†]

[†]Department of Chemical Engineering, National Taiwan University, Taipei 10617, Taiwan

[‡]Department of Organic Device Engineering and Research Center for Organic Electronics, Yamagata University, Yonezawa, Yamagata 992-8510, Japan

Supporting Information

ABSTRACT: We report the fabrication and characterization of polymer resistive switching memory devices fabricated from conjugated rod−coil poly[2,7-(9,9-dihexylfluorene)]-*block*-poly(2-vinylpyridine) diblock copolymers (**PF-*b*-P2VP**) and their hybrids with [6,6]-phenyl-C_{61}-butyric acid methyl ester (PCBM). **PF_{10}-*b*-$P2VP_{37}$** and **PF_{10}-*b*-$P2VP_{68}$**-based devices exhibited the volatile static random access memory (SRAM) characteristic with an ON/OFF current ratio up to 1×10^7, which was explained by the trapping/back transferring of charge carrier. **PF_{10}-*b*-$P2VP_{68}$** had a longer holding time in the ON state than **PF_{10}-*b*-$P2VP_{37}$** because of the delayed back transfer of trapping carriers originally from the longer **P2VP** blocks. The PCBM aggregated size in the composite thin films were effectively reduced by **PF-*b*-P2VP** compared to the homopolymer of **PF** or **P2VP**, because of the supramolecular charge transfer interaction, as evidenced by absorption and photoluminescence spectra. Their PCBM/**PF-*b*-P2VP** composite devices changed from the nonvolatile write-once-read-many-times (WORM) memory to the conductor behavior as the PCBM composition was increased. The electric-field induced charge transfer effect enabled the electrical bistable states for the applications in digital WORM memory device. The tunable memory characteristics through the block length ratio of block copolymers or PCBM composition provided the solution-processable charge storage nanomaterials for programmable high density memory device with a reducing bit cell size.

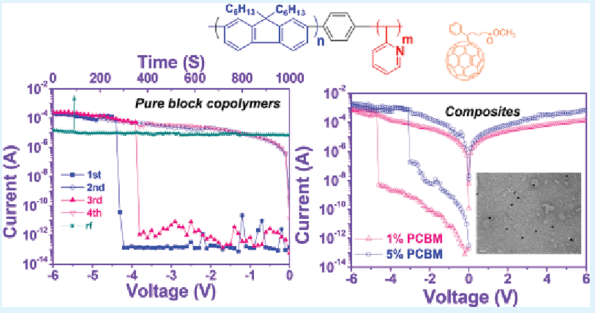

KEYWORDS: memory, block copolymers, fullerene, composite, resistive switching, rod−coil

INTRODUCTION

Organic polymer-based electrical bistable devices have been extensively studied because of their advantages of structural flexibility, low fabrication cost, printability, and three-dimensional stacking capability.[1−6] The OFF and ON states of the memory devices are determined by the switching response between low and high conductance modulated through external electric field. Polymeric materials that exhibit conductance switching phenomena include conjugated polymers,[7−9] functional polyimides (PIs),[10−12] polymers with pendent electroactive chromophores,[13−15] and polymeric composites.[16−28] The switching mechanism on the bistability is explained on the basis of electric field induced transfer of charge carriers,[10−12,16−19,26−28] charge trapping/detrapping,[7−9,14,15,21−23] filament formation,[20] and tunneling effect,[24,25] etc. Single polymers exhibit good solution processability and thermal stability that are selected as memory materials with the simplicity of sandwiched device structures.[7−15] In addition, hybrid composite materials containing filled additives (metal nanoparticles (NPs)[16−20] or fullerene derivatives[21−28]) embedded in the supporting polymer matrices can also be used to induce the bistable resistive switching. The composition and aggregated domain size of the guest additives within the host polymer are the keys to their memory characteristics.

Conjugated rod−coil block copolymers provide a powerful route toward supramolecular objects with the self-organizied structures and specific physical properties.[29] The $\pi-\pi$ interaction between conjugated rods give the additional structural control factor and functionality for the applications on organic electronics. Polyfluorene-based copolymers with metal complex[30] or organic acceptors[7,8,21] were indentified for promising memory applications due to the good electron donating fluorene moieties and good thermal robust stability. For example, Ikkala and his coworkers discovered the negative differential resistance (NDR) characteristics from the memory device based on polystyrene-*block*-poly(9,9-di-n-hexyl-2,7-fluorene)-*block*-polystyrene (PS-*b*-PDHF-*b*-PS) coil−rod−coil triblock copolymer.[31] Our groups also demonstrated that regioregular poly(3-hexylthiophene) (**P3HT**)-*block*-poly(2-phenyl-5-(4-vinylphenyl)-1,3,4-oxadiazole) (**POXD**) rod−coil diblock copolymers exhibited nonvolatile

Received: September 3, 2011
Accepted: October 17, 2011
Published: October 17, 2011

memory behavior through controlling morphology and physical interaction of each block.[9] It suggests that switching behavior triggered by electric field can be determined from structural blocks with electric functionalities and corresponding morphology.

The design and fabrication of nanostructured materials are expected to be as an advanced high-density memory based on nanoscale element cells.[5] Block copolymers that consist of two or more covalently bonded blocks could produce various morphologies depending on the nature of block copolymers (block ratio or structures)[32,33] and are emerging as a promising class of materials for controlling process associated with (opto-) electronics either as semiconductors or structure directors.[34,35] They can also be used to effectively disperse fillers and prevent its aggregation for electrical memory device applications.[18,36−39] Leong et al. first demonstrated the versatility of using self-assembled PS-*b*-P4VP block copolymers with in situ synthesis of Au nanoparticles (NPs) for polymer memory fabrication, in which capacitance−voltage or current−voltage hysteresis represented the charge confinement in the embedded Au NPs.[36−38] De Rosa et al. selectively included NPs in target domains of the long-range ordered coil−coil block copolymers for positioning of NPs on the high-density memory device application.[18] Multilevel data storage through highly ordered block copolymer arrays of metallic NPs as charge trapping element could be realized by utilizing the saturation of programmed/erased states.[39] However, electrical switching behavior based on conjugated rod−coil block copolymers and their composite films have not been fully explored yet.

In this study, we report the resistive memory device characteristics based on the supramolecular materials of poly[2,7-(9,9-dihexylfluorene)]-block-poly(2-vinylpyridine) (**PF-*b*-P2VP**) and their corresponding hybrids with [6,6]-phenyl-C_{61}-butyric acid methyl ester (PCBM). The morphologies, properties, and memory device characteristics of two asymmetric diblock copolymers, **PF_{10}-*b*-$P2VP_{37}$** and **PF_{10}-*b*-$P2VP_{68}$**, were studied. Besides, the domain size of PCBM molecules could be reduced through the charge transfer interaction of the fluorene/2-vinylpyridine and PCBM or block copolymer micellar morphology. The **PF-*b*-P2VP**/ PCBM composite thin films between ITO and Al electrodes were used as the active memory layer for comparison. Finally, the electrical characteristics were analyzed by the appropriate model and the switching mechanisms were proposed for our fabricated resistive switching materials.

EXPERIMENTAL SECTION

Materials. The **PF-*b*-P2VP** rod−coil diblock copolymers were prepared by combining typical coupling reaction and living anionic polymerization as reported by us,[40] which named as **PF_{10}-*b*-$P2VP_{37}$**(M_n = 8.4 kg mol^{-1}, M_w/M_n = 1.89) and **PF_{10}-*b*-$P2VP_{68}$**(M_n = 10.7 kg/mol, M_w/M_n = 2.11). The homopolymers, poly(9,9-di-n-hexylfluorenyl-2,7-diyl) (**PF**; M_n = 3.40 kg/mol) and poly(2-vinyl pyridine) (**P2VP**; M_n = 14.0 kg/mol, M_w/M_n = 1.05), were purchased from Sigma-Aldrich (St. Louis, MO) and Polymer Source Inc. (Dorval, Canada), respectively. [6,6]-phenyl-C_{61}-butyric acid methyl ester (**PCBM**) was obtained from Nano-C Inc. (Westwood, MA). Solvents chloroform was purchased from Acros Organics (Geel, Belgium). All the chemicals were used as received and without further purification.

Characterization. Thermal analyses were carried out on a differential scanning calorimetry (DSC) from TA Instruments (TA Q100) with heating cycle from −30 to 270 °C at the heating rate of 10 °C/min and a thermal gravimetric analyzer (TGA) from Perkin-Elmer 7 with heating range from 70 to 800 °C at the heating rate of 20 °C/min. UV−vis absorption and photoluminescence (PL) spectra were recorded with Hitachi U-4100 spectrometer and Fluorolog-3 spectrofluorometer (Jobin Yvon), respectively. Electrochemistry was performed with a CHI 611B electrochemical analyzer using an ITO plate as working electrode, platinum wire as counter electrode, and Ag/AgCl as reference electrode at a sweep rate 0.1 V/s. Transmission electron microscopy (TEM) images were obtained with a JEOL JEM-1230 instrument operating at a voltage of 50 kV with a Gatam dual vision CCD camera. The samples for TEM measurement were prepared by spin-coating on 200-mesh copper grids. The morphologies of polymer film surface were also obtained with a Nanoscope 3D Controller atomic force micrographs (AFM, Digital Instruments) operated in the tapping mode. The thickness of polymer film was measured with a Microfigure Measuring Instrument (Surfcorder ET3000, Kosaka Laboratory Ltd.).

Device Fabrication and Measurement. The memory devices were fabricated on the indium−tin oxide (ITO) coated glass, with a configuration of ITO/polymers/Al. Before the fabrication of the polymer layer, the glass was precleaned by ultrasonication with deionized water, acetone, and isopropanol each for 20 min, respectively. Then, 10 mg/mL of block copolymers containing 0−7% PCBM (relative to the weight of block copolymers) in chloroform were first filtered through 0.45 μm pore size of PTFE membrane syringe filter. The filtered solution was spin-coated onto the precleaned ITO glass at a speed rate of 1500 rpm for 60 s. Thin films were dried under a vacuum for 10 min to remove the residual solvents. The polymer film thickness was determined to be around 100 nm. Finally, a 300-nm-thick Al top electrode (recorded device units of 0.5 × 0.5 mm^2 in size) was thermally evaporated through the shadow mask at a pressure of 1×10^{-7} Torr with a uniform depositing rate of 1−2 Å/s. The electrical characterization of the memory device was performed by a Keithley 4200-SCS semiconductor parameter analyzer equipped with a Keithley 4205-PG2 arbitrary waveform pulse generator. ITO was used as the cathode and Al was set as the anode during the voltage sweep with a step of 0.1 V. The probe tip used 10 μm diameter tungsten wire attached to a tinned copper shaft with a point radius <0.1 μm (GGB Industries, Inc.). All of the electronic measurements were performed in a N_2-filled glovebox.

RESULTS AND DISCUSSION

The synthesized **PF-*b*-P2VP** block copolymers show good solution processability and are easily fabricated by spin-coating with high-quality thin films. Thermal properties of the copolymers are investigated by TGA and DSC and shown in Figure S1 of the Supporting Information. The thermal decomposition temperatures (T_d, 5% weight-loss) are found at the range of 343−352 °C under flowing nitrogen atmosphere. The glass transition peaks are observed at 84.6 and 81.6 °C for **PF_{10}-*b*-$P2VP_{37}$** and **PF_{10}-*b*-$P2VP_{68}$**, respectively. The good thermal stability of block copolymers backbones confirms their heat resistance for electronic device.

The optical absorption spectra of block copolymers thin films are shown in Figure S2 of Supporting Information. The main absorption peaks of the block copolymer thin films are identified by a linear superposition of the absorption on **PF** and **P2VP** homopolymers. Both **PF_{10}-*b*-$P2VP_{37}$** and **PF_{10}-*b*-$P2VP_{68}$** films exhibit the maximum absorption peak at 375 nm, reflecting the status of the $\pi-\pi^*$ transition of the conjugated fluorene rod moieties.[40] The slightly red-shifted absorption maximum and increase in absorption edge of the **PF-*b*-P2VP**block copolymers thin films compared to **PF** homopolymer reveal the better interchain interaction of the former. The optical band gaps of **PF_{10}-*b*-$P2VP_{37}$** and **PF_{10}-*b*-$P2VP_{68}$** estimated from the onset

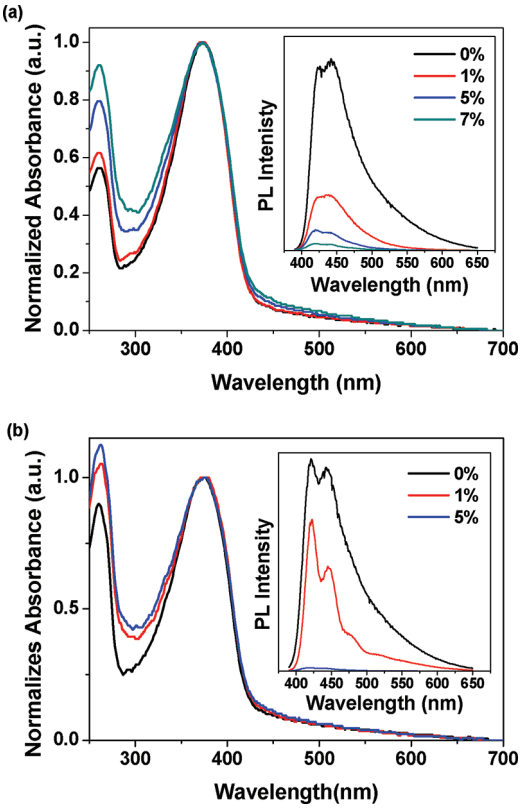

Figure 1. Optical absorption and photoluminescence (PL) spectra of (a) PCBM:**PF$_{10}$-*b*-P2VP$_{37}$**, and (b) PCBM:**PF$_{10}$-*b*-P2VP$_{68}$** thin films.

absorbance are 2.96 and 2.95 eV, respectively. Figure S3 in Supporting Information shows the cyclic voltammagrams (CV) of the studies polymer thin films in a 0.1 M tetrabutylammonium perchlorate (TBAP)/acetonitrile solution at a sweeping rate of 100 mV/s. The energy level of the HOMO was determined from the onset oxidation, assuming that the absolute energy of the level of Fc/Fc$^+$ is 4.8 eV below a vacuum. The HOMO energy levels for **PF$_{10}$-*b*-P2VP$_{37}$** and **PF$_{10}$-*b*-P2VP$_{68}$** are estimated to be −5.57 and −5.64 eV, respectively. Besides, the LUMO level of **PF$_{10}$-*b*-P2VP$_{37}$** and **PF$_{10}$-*b*-P2VP$_{68}$** are −2.62 and −2.69 eV, respectively, which are estimated from the difference between HOMO level and optical band gap. The HOMO level of block copolymers is enhanced with increase in the electron-donating fluorene chain length.

For the case of **PF$_{10}$-*b*-P2VP$_{37}$**:PCBM, as the PCBM composition is increased from 0% to 7%, the absorbance edge of thin film states slightly increases in the range of 420−550 nm (Figure 1a) and the color of solution mixture turns to brown resulted from the charge transfer complexation between **P2VP** blocks and **PCBM**. Similar spectral changes occur in **PF$_{10}$-*b*-P2VP$_{68}$** hybrid with PCBM (Figure 1b), which is consistent with that of PCBM:poly(4-vinypyridine) (**P4VP**) reported in the literature.[41] In this case, **P2VP** blocks are also expected to have a strong tendency to interact with PCBM, which gives better compatibility in terms of electronic properties. The interaction between block polymers and PCBM is further detected by the photoluminescence (PL) spectra of the composite thin films as shown in the inset of Figure 1. The emission spectra are obtained with the excitation wavelength of 370 nm. The PL spectrum of the pristine **PF$_{10}$-*b*-P2VP$_{37}$** thin film exhibits strong well-resolved

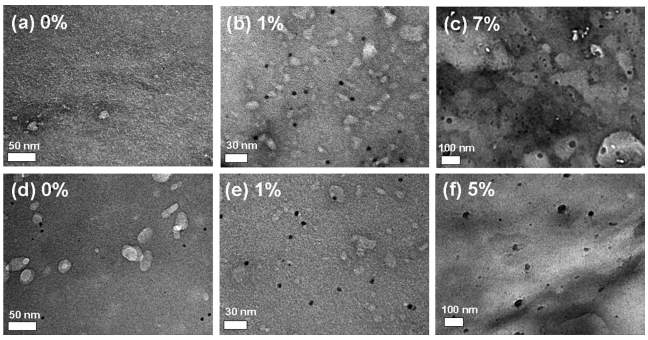

Figure 2. TEM plane view images of (a) **PF$_{10}$-*b*-P2VP$_{37}$**, (b) 1% PCBM:**PF$_{10}$-*b*-P2VP$_{37}$**, (c) 7% PCBM:**PF$_{10}$-*b*-P2VP$_{37}$**, (d) **PF$_{10}$-*b*-P2VP$_{68}$**, (e) 1% PCBM:**PF$_{10}$-*b*-P2VP$_{68}$**, and (f) 5% PCBM:**PF$_{10}$-*b*-P2VP$_{68}$** thin films.

vibronic emission peaks located at 426 and 442 nm and broad emission extended into higher wavelengths due to the aggregated conjugated chain. However, the emission is almost quenched by adding 7% PCBM, which is also probably due to charge transfer. The blending of the **PF$_{10}$-*b*-P2VP$_{68}$** block copolymer with PCBM gives rise to the further quench and reduces in luminescence of the PL from the neat copolymer thin film to the 5% PCBM blend. In indicates that the block copolymers can interact with PCBM probed by both absorption and PL spectra. The complete PL quenching in the blend film suggests that the exciton dissociation in the block copolymers/PCBM system is efficient and photogenerated excitons can not be easily recombined.

The morphologies of the block copolymers and their hybrid composite thin films are analyzed by AFM (see Figure S4 in the Supporting Information) and TEM (Figure 2) image. Thin films are determined to be smooth in the ITO substrate with a 2−3 nm root-mean-square (rms) surface roughness from the AFM analysis. The TEM image shows that pure block copolymers exhibit disordered micellar microstructures (Figure 2a, d) and the PCBM molecules are well-dispersed in block copolymer matrix. The domain size of PCBM in block copolymer matrix estimated from the dark domains is around 10−30 nm (Figure 2b, e), which is much smaller than the PCBM aggregated clusters in **PF** and **P2VP** matrix (more than 150 nm, see Figure S5 in the Supporting Information). It suggests that the charge transfer between the **P2VP** segments and PCBM, and microphase separation of block copolymers reduce the PCBM domain size through the interaction. The good dispersion of PCBM molecules in block copolymers is recognized to form the transition of stable high conductance electron channel. Such difference on PCBM domain size varies the switching characteristic as discussed in the following section.

The electrical behaviors are tested by the current−voltage (I−V) characteristics and constructed using the block copolymers and their composite thin film in a trilayer device. Here, the block length and PCBM loading content on the electrical performance of the device are systematically investigated. The typical I−V characteristics of the memory devices fabricated with **PF$_{10}$-*b*-P2VP$_{37}$** and **PF$_{10}$-*b*-P2VP$_{68}$** in steps of 0.1 V are shown in panels a and b in Figure 3, respectively. For the case of pure **PF$_{10}$-*b*-P2VP$_{37}$**, the device starts with low conductivity OFF state ("0" signal in data storage) and the current increases slowly as the voltage sweeps from 0 to −4 V. The current keeps low until

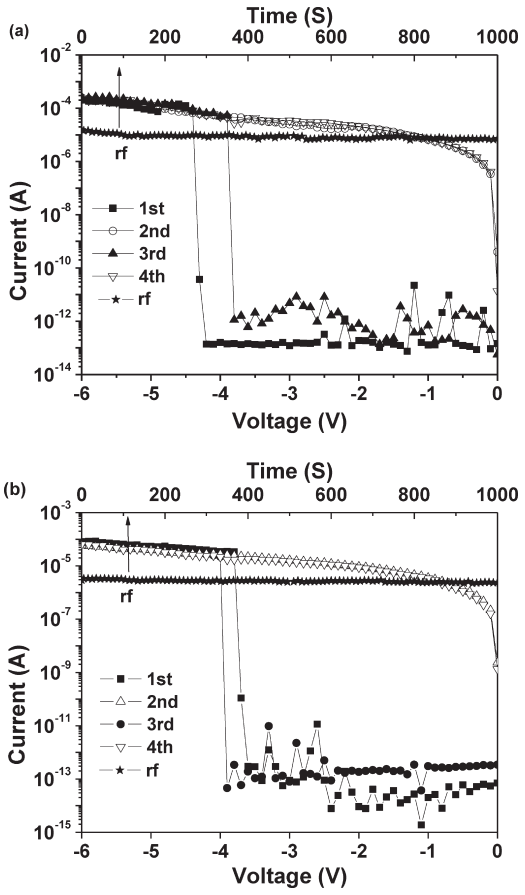

Figure 3. *I*−*V* characteristics of (a) ITO/$\mathbf{PF_{10}}$-*b*-$\mathbf{P2VP_{37}}$/Al and (b) ITO/ $\mathbf{PF_{10}}$-*b*-$\mathbf{P2VP_{68}}$/Al devices.

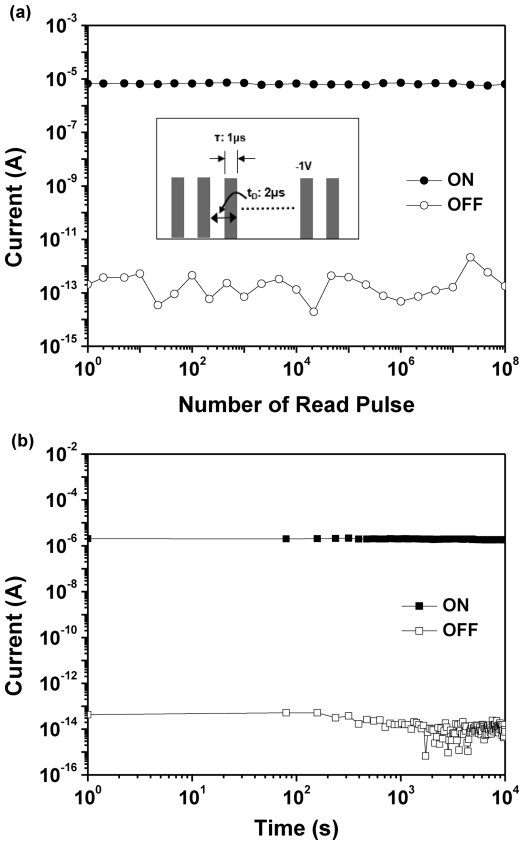

Figure 4. Stability tests for the ITO/$\mathbf{PF_{10}}$-*b*-$\mathbf{P2VP_{37}}$/Al device. (a) Stimulus effect of read pulses on the ON and OFF states at a read voltage of −1.0 V. The inset shows the pulse shapes in the measurement. (b) Retention times on the ON and OFF states under a continuous readout voltage (−1.0 V).

the turn-ON voltage. At threshold voltage (−4.2 V), an abrupt current jump occurs from 10^{-13} to 10^{-4} A (first sweep) indicating that the transition from the low-conductance OFF state to the high-conductance ON state ("1" signal in data storage). The electronic transition is equivalent to the "writing" process in the digital memory cell and the $\mathbf{PF_{10}}$-*b*-$\mathbf{P2VP_{37}}$ device exhibits the distinctly bistable conductance state with an ON/OFF current ratio up to 10^7 which leads to a low misreading rate for memory applications. After reading the ON state during the subsequent sweep from 0 to −6 V (second sweep), the device with sufficient magnitude of −3.8 V can be reprogrammed from the OFF to ON state which is conducted after removing the power. The OFF state can be further recovered to a stored state again with a reapplied switching voltage bias indicating that thin device is rewritable (third sweep). The ON state can be maintained for approximately 5 min after the removal of power and would gradually relax back to the initial OFF state on the continuous repeated sweep cycle. Based on the electrical switching behavior, it can be concluded that the $\mathbf{PF_{10}}$-*b*-$\mathbf{P2VP_{37}}$ memory device still exhibits the volatile nature of a static random access memory (SRAM) since the stored data are finally lost. The volatile $\mathbf{PF_{10}}$-*b*-$\mathbf{P2VP_{37}}$ has a repeated operation and good accuracy for at least 15 different cells. In addition, the unstable ON state of the volatile memory device can also be retained by a refreshing voltage pulse of −1 V within 1 ms duration every 5 s (named as the rf trace). The long-term stability and endurance are also evaluated from the retention time test under voltage stress and stimulus effect of read pulse (Figure 4). Initially, the memory device starts to turn ON or OFF to a high or low conductivity states, respectively and the retention time tests under a constants stress of 1 V of both the ON and OFF states of $\mathbf{PF_{10}}$-*b*-$\mathbf{P2VP_{37}}$ device are evaluated. An ON/OFF current ratio of 1×10^7 to 1×10^8 can be maintained and no obvious current degradation is observed for both the ON and OFF states as functions of the retention time for at least 10^4 s. The stimulus effect of read pulses uses a pulse voltage (pulse width of 1 μs and pulse period of 2 μs, respectively) without significant change in the ON and OFF state current for more than 1×10^8 continuous pulse cycles. However, as the **P2VP** moieties increases, the $\mathbf{PF_{10}}$-*b*-$\mathbf{P2VP_{68}}$ device also reveals similar volatile nature of switching characteristics (Figure 3(b)). The main difference between these two block copolymers lies in slightly longer period time for the retained ON state of the $\mathbf{PF_{10}}$-*b*-$\mathbf{P2VP_{68}}$ device (about 10 min). A pulse endurance of 10^8 times and retention ability of $\mathbf{PF_{10}}$-*b*-$\mathbf{P2VP_{68}}$ device converges to an ON/OFF current ratio of 1×10^7 (see Figure S6 in the Supporting Information). Tests on the devices based on homopolymers, **PF** and **P2VP**, are also carried out as a reference. The device fabricated from the **PF** hompolymer as active layer shows only moderately high conductance state without bistability behavior while the **P2VP** device exhibits a low current in the range of 1×10^{-13} to 1×10^{-10} A even with the high external applied voltage due to its insulating nature (see Figure S7 in the

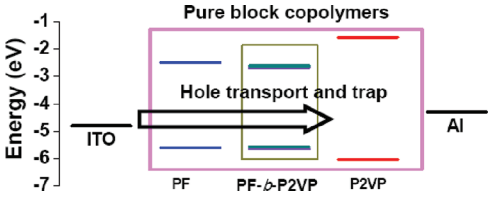

Figure 5. Energy diagram and operation mechanism of ITO/**PF**-*b*-**P2VP**/Al device.

Supporting Information). It confirms the good hole-transporting properties based on conjugated **PF** homopolymer.

The volatile block copolymers device may be explained from the formation of trapping level in the device. It can be rationalized by evaluating the HOMO and LUMO energy levels of polymers combined with work function of ITO and Al electrode, as shown in Figure 5. Note that there is no obvious charge transfer interaction between **PF** and **P2VP** blocks from absorption and CV results. In ITO/pure block copolymers/Al device, the energy barrier for hole injection (HOMO level of polymers/ITO contact) is much smaller than for electrode injection (LUMO level of polymers/Al contact). Thus, it is easier for current flow when the ITO is enriched with holes (the top electrode is applied with negative bias). **PF** block is the dominated component and acts a hole-transport media and p-type semiconductor since PF displays single state conductor behavior whereas **P2VP** block is likely to serve as the hole-blocking moieties in active layer due to its low-lying HOMO level. Upon applying negative voltage bias to Al electrode, holes are injected from ITO into the memory layer, trapped by the PF block and accumulated at trapping sites. At the threshold voltage, charge trapping sites are filled and holes obtain sufficient energy to be escaped from the captured **PF** condition. Therefore, the device switches from the OFF to ON state with a trap-free environment. The trapped holes may be redistributed or back transferred along the **PF** without a continuous voltage bias which leads to the volatile nature. The slightly longer holding period during the ON state and smaller threshold voltage of $\mathbf{PF_{10}}$-*b*-$\mathbf{P2VP_{68}}$ device than those of $\mathbf{PF_{10}}$-*b*-$\mathbf{P2VP_{37}}$ device are probably due to the obvious trapping conditions and difficult effective charge hopping originally from the longer block length of **P2VP**.

Besides, the *I*−*V* characteristics of the hybrid composites device are investigated as a function of PCBM composition in the block copolymer matrix as shown in Figure 6. The thicknesses of block copolymers composite thin film are adjusted to be similar to that of pristine block copolymers active layer while varying the PCBM composition. At low PCBM content (1 or 5%) in $\mathbf{PF_{10}}$-*b*-$\mathbf{P2VP_{37}}$ composite (Figure 6(a)), the voltage applied to the device is scanned in a cycle from 0 to −6 V (first sweep); 0 to −6 V (second sweep); 0 to 6 V (third sweep). Starting with the low conductivity state (OFF state) in the device, the current increases abruptly and the device has a transition to ON state at the threshold voltage of −4.6 V for 1% PCBM device and −3 V for 5% PCBM device, respectively. After the transition is achieved, the ON state is maintained in the device (second sweep) even after the power is turned off or by applying a reverse bias voltage (third sweep), thereby suggesting the nonvolatile write-once-read-many-times (WORM) memory behavior. Although the *I*−*V* curves for 5% PCBM device show a larger ON and OFF state current, the current ratio between ON and OFF states for 1% PCBM device is as large as about 1×10^6 at −1 V, which is

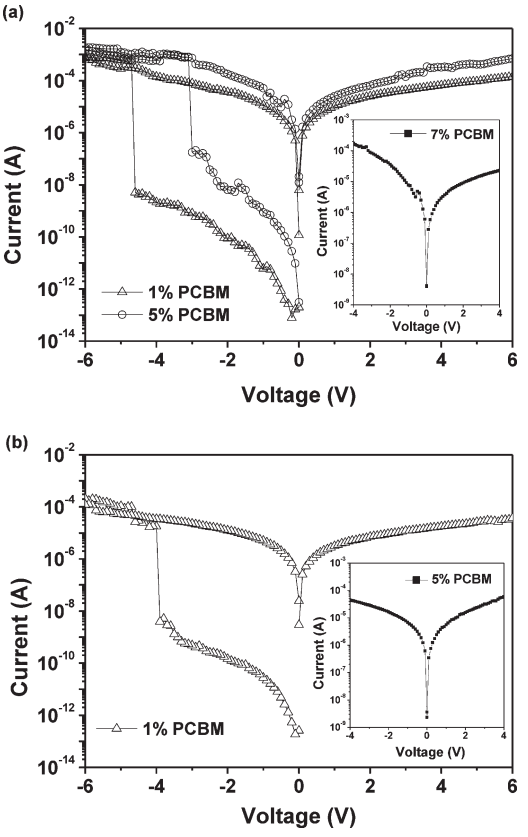

Figure 6. *I*−*V* characteristics of (a) ITO/PCBM:$\mathbf{PF_{10}}$-*b*-$\mathbf{P2VP_{37}}$/Al and (b) ITO/PCBM:$\mathbf{PF_{10}}$-*b*-$\mathbf{P2VP_{68}}$/Al devices.

two orders higher than 5% PCBM device. As the loading ratio of PCBM molecules gets higher, the threshold voltage decreases obviously for WORM device. Both ON state and OFF state current of the WORM device can be sustained for up to 1×10^4 s and 1×10^8 continuous read pulsed of −1 V as shown in Figures S8 and S9 in the Supporting Information. With further increase in PCBM loading ratio up to 7%, the composite film exhibits only a single state as a conduction characteristic. The *I*−*V* curves for PCBM:$\mathbf{PF_{10}}$-*b*-$\mathbf{P2VP_{68}}$ devices also show manifestly essential electrical features based on the PCBM composition (Figure 6b). For comparison, 1% PCBM:$\mathbf{PF_{10}}$-*b*-$\mathbf{P2VP_{68}}$ device has a WORM memory with a reduced threshold voltage of −3.9 V and 5% PCBM device directly short-circuits the current pathway. The stability tests of 1% PCBM:$\mathbf{PF_{10}}$-*b*-$\mathbf{P2VP_{68}}$ WORM-type memory device are demonstrated in Figure S10 in the Supporting Information. In summary, the electrical properties of PCBM:block copolymers composite device change from volatile behavior (without PCBM) to nonvolatile WORM memory and conductor as the PCBM composition increases.

The switching behavior of block copolymer:PCBM composite WORM memory devices is proposed in terms of charge transfer state between block copolymers (electron donor) and PCBM (electron acceptor) under an applied voltage,[26−28] and the relative energy diagram is shown in Figure 7. These interactions keep the PCBM molecules from aggregation and the memory characteristics occurs in prepared composite thin film. Initially, the device remains the low conductance state under the low voltage of first negative sweep because of the energy barriers for the hole injection from ITO or electron injection from Al to

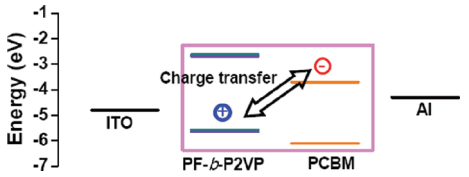

Figure 7. Energy diagram and operation mechanism of ITO/PCBM: **PF**-*b*-**P2VP**/Al device.

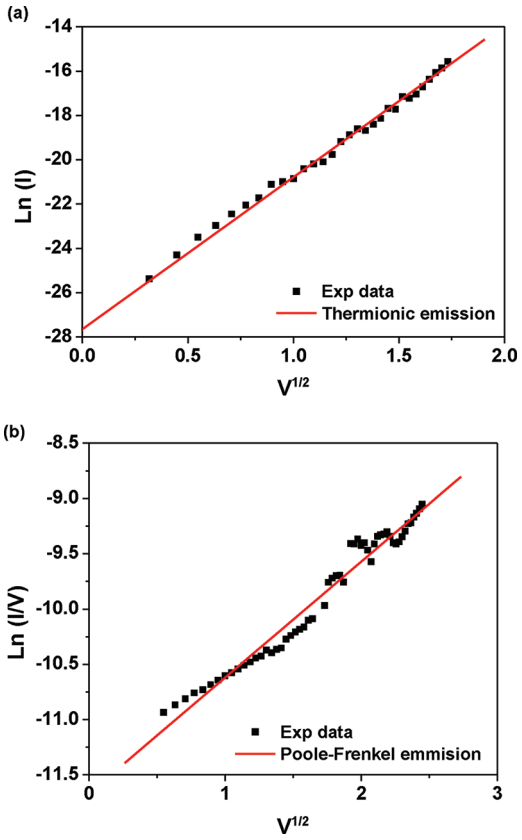

Figure 8. Analysis on fitted $I-V$ characteristics of the ITO/5% PCBM: $\mathbf{PF}_{10}$-*b*-$\mathbf{P2VP}_{37}$/Al device in the (a) OFF state and (b) ON state.

polymer thin films. Charge transfer interaction can not be occurred in ground state from the original corresponding energy level. However, when the voltage sweeps above the threshold voltage, electron can be transferred from the HOMO level of block copolymers donors to the LUMO level of PCBM acceptors and give rise to an abrupt increase in the current response. PCBM molecules exhibit the electron-accepting behavior by exchanging electrons with electron donors to form the corresponding negatively charged counterions with the noncovalent interaction. The stabilized charge transfer state may not easily be recombined even under the reversed bias and the ON state is thus retained for a long time in the observed WORM memory device. The switching phenomenon based on charge transfer interaction between fluorene based block copolymers and PCBM is proved by the PL quenching with the decay of photogenerated exciton.[27,28,42] Since the overlap between emission spectrum of block copolymers and absorption spectrum of PCBM is rather small, the resonance energy transfer between them can be neglected. The morphology of PCBM molecules in the block

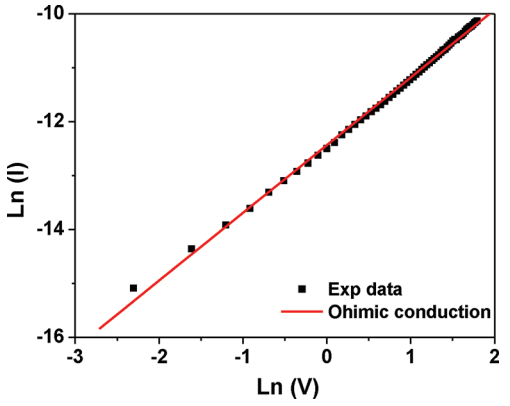

Figure 9. Analysis on fitted $I-V$ characteristics of the ITO/7% PCBM: $\mathbf{PF}_{10}$-*b*-$\mathbf{P2VP}_{37}$/Al device in the ON state.

copolymers plays a crucial role in the performance of memory device. The loading ratio of PCBM allows the device to manipulate the electrical characteristics since the PCBM domain can be controlled through the PCBM distribution in the microphase-separated block copolymers matrix. With a further increase in PCBM composition, a small increase in PCBM size (or reduce in distance between the isolated PCBM domains) is observed from TEM image that exhibits smaller threshold voltage and ON/OFF current ratio of 5% PCBM:$\mathbf{PF}_{10}$-*b*-$\mathbf{P2VP}_{37}$ device than those of 1% PCBM:$\mathbf{PF}_{10}$-*b*-$\mathbf{P2VP}_{37}$ device. The energy barrier for the charge transport decreases with the increase in the PCBM composition of the composites and more effective charge transfer conduction channel can be formed in the memory layer.

The obtained I−V curves of WORM composite device (1% or 5% PCBM:$\mathbf{PF}_{10}$-*b*-$\mathbf{P2VP}_{37}$ and 1% PCBM:$\mathbf{PF}_{10}$-*b*-$\mathbf{P2VP}_{68}$) are analyzed with appropriate theoretical conduction models (Figure 8 and Figures S11 and S12 in the Supporting Information) to clarify the carrier transport and mechanism using thermionic emission limited conduction and Poole-Frenkel emission model.[26,43] For the WORM-type composite memory device, the OFF state current below the threshold voltage might be attributed to the thermally generated charge carriers through the straight line fit on the plot of $\ln(I)$ versus $V^{1/2}$. When in high conductance state at positive or negative voltage bias, the ON state currents show a linear fitting plot of $\ln(I/V)$ versus $V^{1/2}$ based on the Poole−Frenkel emission model. However, the characteristics of high current state in 7% PCBM:$\mathbf{PF}_{10}$-*b*-$\mathbf{P2VP}_{37}$ and 5% PCBM:$\mathbf{PF}_{10}$-*b*-$\mathbf{P2VP}_{68}$ device completely show an ohmic current (Figure 9 and Figure S13 in the Supporting Information) and electrically connected channel between two electrodes directly dominates the conducting behavior probably due to the large PCBM domain size (about 80 nm).

From systematic electrical characterization and analysis, the **PF**-*b*-**P2VP** block copolymers and their PCBM blended composites can be addressed as tunable electrical switching materials. Bistable memory behaviors based on pure **PF**-*b*-**P2VP** copolymers are expected to depend on the **PF** transport ability with a coexisting charge trapping environment as copolymerization with second **P2VP** block, and the memory performance is related to the block ratio of **PF**/**P2VP**. Controlling the physical interaction between block copolymers and PCBM changes the device performance to nonvolatile WORM memory or conductor. The reproducible results can be achieved in these memory materials through the choice of polymer backbones, PCBM

composition, and morphology by the supramolecular approach of composite film.

CONCLUSION

We have demonstrated the tunable electrical switching properties with conjugated rod−coil block copolymers and their PCBM blended composites as active layer in resistive memory device. Through tuning the **PF**/**P2VP** block ratio and controlling the PCBM composition and domain size show the distinct electrical effects such as bistable switching and conductor. The memory devices exhibit repeatable volatile SRAM (pure block copolymers) and nonvolatile WORM (block copolymers:PCBM composite) bistable characteristics with high ON/OFF ratio and electrical bistability. The volatile nature of block copolymers device is mainly attributed to the back transferring of shallow traps based on the good transport ability of **PF** block with coexisting **P2VP** block. However, the charge transfer interaction in the block copolymers composite is responsible for the WROM memory effect, as evidenced by the emission and absorption spectrum. The study demonstrates that the block copolymer: PCBM composite materials might have the potential applications for the advanced memory devices by tailoring block ratio or PCBM composition.

ASSOCIATED CONTENT

Supporting Information. Thermal, optical, and electrochemical properties of block copolymers. AFM images of block copolymers and their composites. TEM image of **PF** or **P2VP** hompolymer with PCBM. *I*−*V* characteristics of ITO/**PF** or **P2VP** homopolymer/Al devices. Stability tests and analysis of fitted *I*−*V* characteristics of block copolymers and their composites. This material is available free of charge via the Internet at http://pubs.acs.org.

AUTHOR INFORMATION

Corresponding Author

*Address correspondence to Email: chenwc@ntu.edu.tw; TEL: 886-2-2362-8398; FAX: 886-2-2362-3040.

ACKNOWLEDGMENT

W.-C.C acknowledges the financial support from the National Science Council of Taiwan and the Excellence Research Program of National Taiwan University. C.-L.L. thanks the Dissemination of Tenure Tracking System Program of Ministry of Education, Culture, Sports, Science and Technology-Japan for financial support. We also thank for Prof. J. Kido and Prof. Z. Hong (Yamagata University) helpful discussion on memory device.

REFERENCES

(1) Ling, Q.-D.; Liaw, D.-J.; Zhu, C.; Chan, D. S.-H.; Kang, E.-T.; Neoh, K.-G. *Prog. Polym. Sci.* **2008**, *33*, 917–978.
(2) Yang, Y.; Ouyang, J.; Ma, L.; Tseng, R. J. H.; Chu, C. W. *Adv. Funct. Mater.* **2006**, *16*, 1001–1014.
(3) Scott, J. C.; Bozano, L. D. *Adv. Mater.* **2007**, *19*, 1452–1463.
(4) Heremans, P.; Gelinck, G. H.; Muller, R.; Baeg, K.-J.; Kim, D.-Y.; Noh, Y.-Y. *Chem. Mater.* **2010**, *23*, 341–358.
(5) Lee, S.-J. *J. Mater. Chem.* **2011**, *21*, 14097–14112.
(6) Liu, C.-L.; Chen, W.-C. *Polym. Chem.* **2011**, *2*, 2169–2174.
(7) Ling, Q.-D.; Song, Y.; Lim, S.-L.; Teo, E. Y.-H.; Tan, Y.-P.; Zhu, C.; Chan, D. S. H.; Kwong, D.-L.; Kang, E.-T.; Neoh, K.-G. *Angew. Chem., Int. Ed.* **2006**, *45*, 2947–2951.
(8) Zhuang, X.-D.; Chen, Y.; Li, B.-X.; Ma, D.-G.; Zhang, B.; Li, Y. *Chem. Mater.* **2010**, *22*, 4455–4461.
(9) Fang, Y.-K.; Liu, C.-L.; Li, C.; Lin, C.-J.; Mezzenga, R.; Chen, W.-C. *Adv. Funct. Mater.* **2010**, *20*, 3012–3024.
(10) Ling, Q.-D.; Chang, F.-Y.; Song, Y.; Zhu, C.-X.; Liaw, D.-J.; Chan, D. S.-H.; Kang, E.-T.; Neoh, K.-G. *J. Am. Chem. Soc.* **2006**, *128*, 8732–8733.
(11) Kuorosawa, T.; Chueh, C.-C.; Liu, C.-L.; Higashihara, T.; Ueda, M.; Chen, W.-C. *Macromolecules* **2010**, *43*, 1236–1244.
(12) Liu, C.-L.; Kurosawa, T.; Yu, A.-D.; Higashihara, T.; Ueda, M.; Chen, W.-C. *J. Phys. Chem. C* **2011**, *115*, 5930–5939.
(13) Lim, S. L.; Li, N.-J.; Lu, J.-M.; Ling, Q.-D.; Zhu, C. X.; Kang, E.-T.; Neoh, K. G. *ACS Appl. Mater. Interfaces* **2009**, *1*, 60–71.
(14) Fang, Y.-K.; Liu, C.-L.; Chen, W.-C. *J. Mater. Chem.* **2011**, *21*, 4778–4786.
(15) Fang, Y.-K.; Liu, C.-L.; Yang, G.-Y.; Chen, P.-C.; Chen, W.-C. *Macromolecules* **2011**, *44*, 2604–2612.
(16) Ouyang, J.; Chu, C.-W.; Szmanda, C. R.; Ma, L.; Yang, Y. *Nat. Mater.* **2004**, *3*, 918–922.
(17) Wei, D.; Baral, J. K.; Osterbacka, R.; Ivaska, A. *J. Mater. Chem.* **2008**, *18*, 1853–1857.
(18) De Rosa, C.; Auriemma, F.; Di Girolamo, R.; Pepe, G. P.; Napolitano, T.; Scaldaferri, R. *Adv. Mater.* **2010**, *22*, 5414–5419.
(19) Baker, C. O.; Shedd, B.; Tseng, R. J.; Martinez-Morales, A. A.; Ozkan, C. S.; Ozkan, M.; Yang, Y.; Kaner, R. B. *ACS Nano* **2011**, *5*, 3469–3474.
(20) Cho, B.; Kim, T.-W.; Choe, M.; Wang, G.; Song, S.; Lee, T. *Org. Electron.* **2009**, *10*, 473–477.
(21) Liu, G.; Ling, Q.-D.; Kang, E.-T.; Neoh, K.-G.; Liaw, D.-J.; Chang, F.-C.; Zhu, C.-X.; Chan, D. S.-H. *J. Appl. Phys.* **2007**, *102*, 024502.
(22) Liu, G.; Ling, Q.-D.; Teo, E. Y. H.; Zhu, C.-X.; Chan, D. S.-H.; Neoh, K.-G.; Kang, E.-T. *ACS Nano* **2009**, *3*, 1929–1937.
(23) Song, S.; Cho, B.; Kim, T.-W.; Ji, Y.; Jo, M.; Wang, G.; Choe, M.; Kahng, Y. H.; Hwang, H.; Lee, T. *Adv. Mater.* **2010**, *22*, 5048–5052.
(24) Baral, J. K.; Majumdar, H. S.; Laiho, A.; Jiang, H.; Kauppinen, E. I.; Ras, R. H. A.; Ruokolainen, J.; Ikkala, O.; Osterbacka, R. *Nanotechnology* **2008**, *19*, 035203.
(25) Laiho, A.; Majumdar, H. S.; Baral, J. K.; Jansson, F.; Osterbacka, R.; Ikkala, O. *Appl. Phys. Lett.* **2008**, *93*, 203309.
(26) Chu, C. W.; Ouyang, J.; Tseng, H. H.; Yang, Y. *Adv. Mater.* **2005**, *17*, 1440–1443.
(27) Hsu, J.-C.; Liu, C.-L.; Chen, W.-C.; Sugiyama, K.; Hirao, A. *Macromol. Rapid Commun.* **2011**, *32*, 528–533.
(28) Hsu, J.-C.; Chen, Y.; Kakuchi, T.; Chen, W.-C. *Macromolecules* **2011**, *44*, 5168–5177.
(29) Liu, C.-L.; Lin, C.-H.; Kuo, C.-C.; Lin, S.-T.; Chen, W.-C. *Prog. Polym. Sci.* **2011**, *36*, 603–637.
(30) Liu, S.-J.; Lin, Z.-H.; Zhao, Q.; Ma, Y.; Shi, H.-F.; Yi, M.-D.; Ling, Q.-D.; Fan, Q.-L.; Zhu, C.-X.; Kang, E.-T.; Huang, W. *Adv. Funct. Mater.* **2011**, *21*, 979–985.
(31) Vilkman, M.; Solehmainen, K.; Laiho, A.; Sandberg, H. G. O.; Ikkala, O. *Org. Electron.* **2009**, *10*, 1478–1482.
(32) Bates, F. S.; Fredrickson, G. H. *Phys. Today* **1999**, *52*, 32–38.
(33) Hamley, I. W. *The Physics of Block Copolymers*; Oxford University Press: New York, 1998.
(34) Botiz, I.; Darling, S. B. *Mater. Today* **2010**, *13*, 42–51.
(35) Darling, S. B. *Eng. Environ. Sci.* **2009**, *2*, 1266–1273.
(36) Leong, W. L.; Lee., P. S.; Lohani, A.; Lam, Y. M.; Chen, T.; Zhang, S.; Dodabalapur, A.; Mhaisalkar, S. *Adv. Mater.* **2008**, *20*, 2325–2331.
(37) Leong, W. L.; Mathews, N.; Mhaisalkar, S.; Lam, Y. M.; Chen, T.; Lee., P. S. *J. Mater. Chem.* **2009**, *19*, 7354–7361.
(38) Leong, W. L.; Mathews, N.; Tan, B.; Vaidyanathan, S.; Dotz, F.; Mhaisalkar, S. *J. Mater. Chem.* **2011**, *21*, 8971–8974.

(39) Lee, J.-S.; Kim, Y.-M.; Kwon, J.-H.; Sim, J. S.; Shin, H.; Sohn, B.-H.; Jia, Q. *Adv. Mater.* **2011**, *23*, 2064.
(40) Lin, C.-H.; Tung, Y.-C.; Ruokolainen, J.; Mezzenga, R.; Chen, W.-C. *Macromolecules* **2008**, *41*, 8759–8769.
(41) Laiho, A.; Ras, R. H. A.; Valkama, S.; Ruokolainen, J.; Österbacka, R.; Ikkala, O. *Macromolecules* **2006**, *39*, 7648–7653.
(42) Ohkita, H.; Cook, S.; Astuti, Y.; Duffy, W.; Tierney, S.; Zhang, W.; Henney, M.; McCulloch, I.; Nelson, J.; Bradley, D. D. C.; Durrant, J. R. *J. Am. Chem. Soc.* **2008**, *130*, 3030–3042.
(43) Sze, S. M.; Ng, K. K. *Physics of Semiconductor Devices*; Wiley-InterScience: Hoboken, NJ, 2007.